Korean J. Chem. Eng., 39(9), 2513-2522 (2022)
DOI: 10.1007/s11814-022-1106-3

pISSN: 0256-1115
eISSN: 1975-7220

Application of amine-loaded activated carbon fiber in CO_2 capture and separation

Haoran Liu*, Xinmei Lu*, Liying Liu*,†, Jian Wang*, Pengyu Wang, Peng Gao*, Tingsheng Ren*, Guo Tian*, and Di Wang***

*State Environmental Protection Key Laboratory of Eco-Industry, Northeastern University, Shenyang 110819, China
**State Grid Liaoning Electric Power Co., Ltd, Shenyang 110004, China
(*Received 6 December 2021 • Revised 3 March 2022 • Accepted 12 March 2022*)

Abstract−The CO_2 emitted by coal-fired power plants is the main factor leading to global warming, and the capture of CO_2 in the flue gas of power plants is still the main task at this stage. Many adsorbents have been developed to capture CO_2 in high-temperature flue gas, but some materials are complicated to synthesize or the cost is too high. Here, we used low-cost raw materials activated carbon fiber and PEI, and used green synthesis to synthesize new adsorbents in order to capture CO_2 in high-temperature flue gas of a power plant. To improve the performance of highly porous activated carbon fiber (ACF) in CO_2 capture and separation, an organic polymer polyethylenimine (PEI) was loaded successfully into the oxidized ACF. The modified adsorbent was tested by FT-IR, XRD and SEM, and the CO_2 adsorption capacity and CO_2/N_2 selectivity were analyzed. The results showed that the as-synthesized PEI-modified adsorbent has a CO_2 adsorption capacity of 2.5 mmol/g, which is 1.7 times better than that of the pristine ACF adsorbent (1.5 mmol/g), at 1 bar and 333 K, and it has excellent CO_2/N_2 selectivity, as calculated by ideal adsorption solution theory (IAST). These data indicate that PEI was loaded successfully into the oxidized ACF. In addition, the dual site Langmuir isotherm equation and Langmuir isotherm equation can be in good agreement with the adsorption curves of CO_2 and N_2. In comparison with other composite adsorbents, the preparation process of the present new adsorbent is highly environmentally friendly, the synthesis method is simple and the cost is low, which demonstrates potential applications in the separation of CO_2 from the flue gas of power plants.

Keywords: ACF, PEI, CO_2, Capture, Separation

INTRODUCTION

With rapid economic development and the increase in the world's total population, the emission of greenhouse gases has severely affected the balance of the ecosystem, leading to global warming, melting of glaciers, and rising sea levels. At present, the climate change caused by the greenhouse effect has threatened human survival and become a global problem in urgent need of solution.

The main cause of global warming is the massive emission of greenhouse gases. Greenhouse gases mainly include carbon dioxide (CO_2), methane (CH_4), nitrous oxide (N_2O), hydrofluorocarbons (HFCs), perfluorocarbons (PFCs), and sulfur hexafluoride (SF_6). CO_2 accounts for the highest proportion of greenhouse gases emitted, and CO_2 exists in the atmosphere for a long time, so the greenhouse effect caused by CO_2 gas is the most significant [1]. Currently, the world's total carbon dioxide emissions are still rising rapidly, and it is estimated that by 2100, the CO_2 content will increase to 550 ppm, almost double the amount before the industrial revolution [2]. The 2008 Energy Technology Perspectives (ETP) report pointed out that CO_2 emissions in the energy sector in 2050 will increase by 130% compared to the level in 2005. Since the end of the UN Climate Change Conference in Copenhagen in December 2009, countries have pledged to achieve greenhouse gas emission reduction targets. Generally, improvement of energy efficiency, development of renewable energy and utilization of carbon dioxide capture and storage (CCS) technology are the main ways to achieve a low-carbon economy.

To date, carbon dioxide capture mainly includes precombustion capture, oxygen-enriched capture and post-combustion capture [3,4]. Post-combustion capture has always been the most advanced technology among various carbon capture methods [5]. It captures CO_2 in the flue gas emitted by combustion, mainly including cryogenic distillation [6], chemical absorption [7], membrane separation [8] and physical adsorption [9]. At present, the best and most commonly used adsorption method is physical adsorption because it provides superior adsorption capacity, minimal energy consumption, simple design, and selectivity [10,11]. The commonly used physical adsorbents include activated carbon [12], activated alumina [13], zeolite [14], metal organic frameworks [15,16], and polymers. Activated carbon-derived porous carbon-based materials are not only widely used in CO_2 adsorption, but also in catalysis [17]. Literature data show that the above mentioned adsorbents can effectively separate and purify multicomponent mixtures such as CO_2/N_2 and CO_2/CH_4 [18]. Activated carbon fiber (ACF) is the third generation of a new adsorption material after the widely used powdered activated carbon and granular activated carbon. It is made of fibers as the raw material. ACFs have the advantages of a large specific surface area, rich micropores, uniform distribution, fast ad-

†To whom correspondence should be addressed.
E-mail: liuly@smm.neu.edu.cn
Copyright by The Korean Institute of Chemical Engineers.

sorption speed, and few impurities [19,20]. ACF is widely used in wastewater purification, while the application of ACF for CO_2 separation in industrial waste gas is limited because of the limited adsorption capacity and selectivity of activated carbon fibers for CO_2. In terms of wastewater treatment and dye removal, there have been related reports on self-assembled adsorption nanostructures [21,22]. According to related studies, it can be thought of using influential materials to modify or impregnate ACF, which may improve the adsorption of activated carbon fibers. capacity and selectivity. Among various organic amines, such as polyethylene imine (PEI), tetraethylene pentamine (TEPA), ethylene diamine (ED), etc., PEI has garnered great interest due to its high amine density derived from primary, secondary and tertiary amines [23]. In addition, PEI is widely used because of its high reactivity and selectivity with CO_2; at the same time, PEI has good regeneration ability, the regeneration energy consumption of the adsorbent can be reduced, which can greatly increase the amount of CO_2 adsorption in industrial gases [24].

To achieve this basic goal, we used nitric acid and sulfuric acid hydrothermal methods to oxidize the surface of activated carbon fiber (ACF). Then, the acid-treated activated carbon fiber (O-ACF) was modified by different types and different weights of PEI loading. The successful impregnation of PEI in ACF was characterized by methods such as FT-IR, ICP and XRD. The adsorption performance and selectivity of modified activated carbon fiber for CO_2 was studied by a static adsorption method. The adsorption isotherms were fitted by the dual site Langmuir and Langmuir models. To the best of our knowledge, there are few reports on the CO_2 adsorption of PEI-loaded ACFs.

EXPERIMENTAL

1. Material

Activated carbon fiber (ACF) was purchased from Jiangsu Sensen Carbon Industry Technology Co., Ltd., absolute ethanol (CH_3CH_2OH, M. W=46.07, 99.7%) was purchased from Tianjin Beichen Founder Reagent Factory, polyethyleneimine ($(CH_2CH_2NH_2)_n$, M. W=10,000, 99%) was purchased from Shanghai Maclean Biochemical Technology Co., Ltd., and ultrapure water was taken from an Ultrapure laboratory ultrapure water device. The above chemicals were used without further treatment.

2. Methodology

The activated carbon fiber was washed with ultrapure water and then dried in a constant temperature drying oven at 80 °C for 12 hours. The cleaned ACF was placed into a mixture of HNO_3 and H_2SO_4 (1 : 3, V/V), each with a concentration of 5 mol/L, at a temperature of 100 °C and stirred for 3 hours. Then, the ACF was cleaned with a large amount of ultrapure water to pH 7. The sample was dried in a constant temperature drying oven at 80 °C for 12 hours to obtain sample O-ACF. PEI (0.1 g, 0.2 g, and 0.3 g) was added to an appropriate amount of absolute ethanol and stirred vigorously for 30 minutes to fully dissolve PEI in ethanol. Then, 0.5 g of O-ACF was added to the solution and stirred at a speed of 150 revolutions per minute for 6 hours. It was filtered and cleaned with ethanol and finally dried in a vacuum drying oven at 80 °C for 24 hours. Finally, the samples were named as O-ACF-PEI (5 : 1), O-ACF-PEI (5 : 2) and O-ACF-PEI (5 : 3), respectively.

3. Characterization of Adsorbents

The main working principle of phase analysis of X-ray diffraction is to scan the sample through X-rays and analyze the structure of the sample based on the diffraction peaks formed by the diffraction of X-rays and crystal structures. The structural configurations of ACF, O-ACF, and O-ACF-PEI were examined by X-ray powder diffraction (XRD) using Cu-Ka radiation of 40 kV and 40 mA (D8 ADVANCE, German Bruker AXS Co.). The scanning range was 5-60°, and the scanning speed was 8°/min. An ASAP 2460 automatic specific surface area and microporous physical adsorption analyzer produced by Micromeritics of the United States was used to analyze the nitrogen adsorption isotherm (77 K), pore volume and Brunauer Emmett Teller (BET) surface area of the samples. Then, the corresponding data were collected. The porosity parameters were calculated by the pore size distribution curve as described by the Barrett-Joyner-Halenda (BJH) method, whereas the quantification of the volume of micropores was measured by the t-plot method. An Ultra Plus scanning electron microscope analyzer produced by ZEISS, Germany was used in this experiment with a resolution of 1.0 nm, a magnification of 0.2-10 million, and an acceleration voltage of 0.1-30 kV. Pretreatment was performed before testing the samples. In this study, the samples were sprayed with gold before testing. Fourier transform infrared spectrum analysis is used to study the composition and microstructure of materials. The surface bonds among diverse functional groups on ACF, O-ACF, and O-ACF-PEI were analyzed by using a spectrophotometer (Agilent Cary 660, America) that generated Fourier transform infrared (FTIR) spectra in the range of 400-6,000 cm^{-1}.

4. Adsorption Analysis

An ASAP 2460 automatic physical adsorption instrument produced by Micromeritics was used to determine the CO_2 and N_2 adsorption isotherms of the modified adsorbent at different temperatures from 303 to 363 K using a constant temperature bath method, and the adsorption capacity was determined. Before adsorption, the sample was degassed under 393 K vacuum for 3 hours to remove moisture and unnecessary impurities.

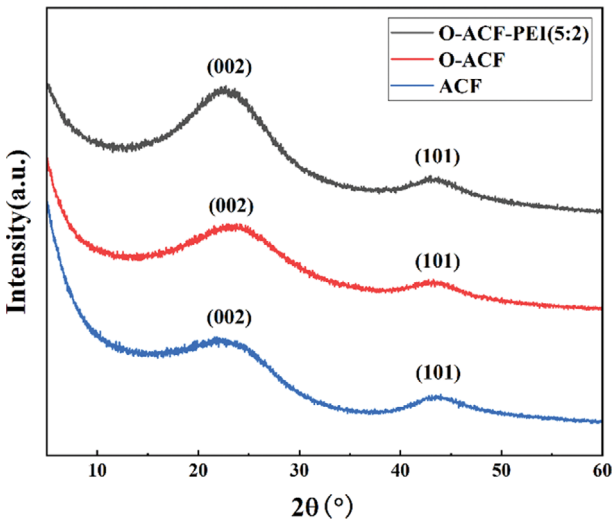

Fig. 1. X-ray powder diffraction analysis of ACF, O-ACF and O-ACF-PEI (5 : 2).

Table 1. The SSA and pore structure characteristics of ACF before and after PEI loading

Samples	BET surface area (m^2/g)	Pore volume (cm^3/g)	Pore size (nm)	Micropore volume (m^3/g)	Mesopore volume (m^3/g)
ACF	1,004.84	0.539	2.14	0.461	0.078
O-ACF	573.44	0.310	2.16	0.257	0.053
O-ACF-PEI (5 : 2)	533.29	0.290	2.17	0.239	0.051

RESULTS AND DISCUSSION

1. Characterization of Materials

The samples were characterized by X-ray powder diffraction. Fig. 1 shows the XRD diffraction patterns of ACF, O-ACF, and O-ACF-PEI (5 : 2). The XRD analysis shows that ACF has two characteristic diffraction peaks at around 2θ=23 degrees and 43 degrees, which correspond to the graphite crystal planes (002) and (100) of carbon materials, respectively. The peak shapes are broad, indicating that ACF is amorphous. In addition, the XRD patterns of O-ACF and O-ACF-PEI (5 : 2) were fundamentally identical. This suggests that the amorphous structure of ACF was well maintained even after oxidation and loading of PEI. Here, the undamaged ACF structure after PEI impregnation shows special resistance to basic amines. However, a slight increase in the sharpness of the characteristic peaks of O-ACF-PEI can also be noticed, which may be attributed to the strong binding of polyethyleneimine molecules to ACF.

The pore structures of ACF, oxidized O-ACF and the sample with PEI loaded were analyzed by the nitrogen adsorption method. In Table 1, we can see that the original ACF has a high specific surface area of 1,004.8 m^2/g and a large pore volume of 0.54 cm^3/g, with an average pore size of 2.1 nm. After loading PEI, due to the filling of PEI molecules, the specific surface area decreased to 573.4 m^2/g and further to 558.5 m^2/g, which may be due to the deposition of PEI molecules in the framework of the adsorbent (ACF). As shown in Fig. 2, all samples exhibited type I isotherms. According to the classification of the International Union of Applied Chemistry (IUPAC), the prepared adsorbents ACF, O-ACF, and O-ACF-PEI show type I adsorption curves. Fig. 2 shows that a large vol-

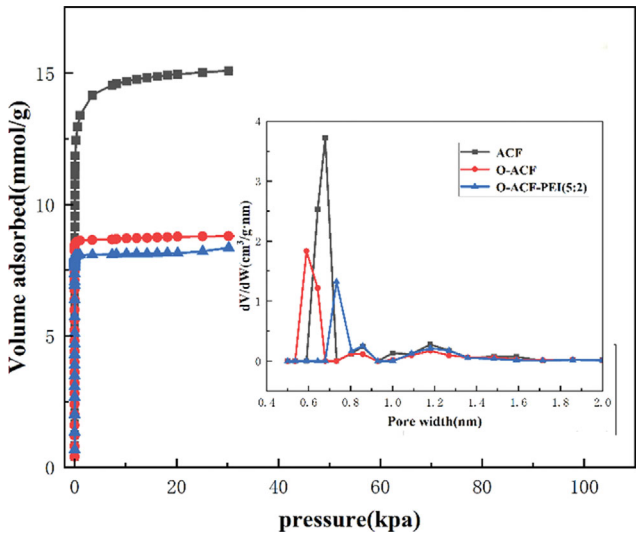

Fig. 2. N_2 adsorption desorption and pore size distribution of prepared samples.

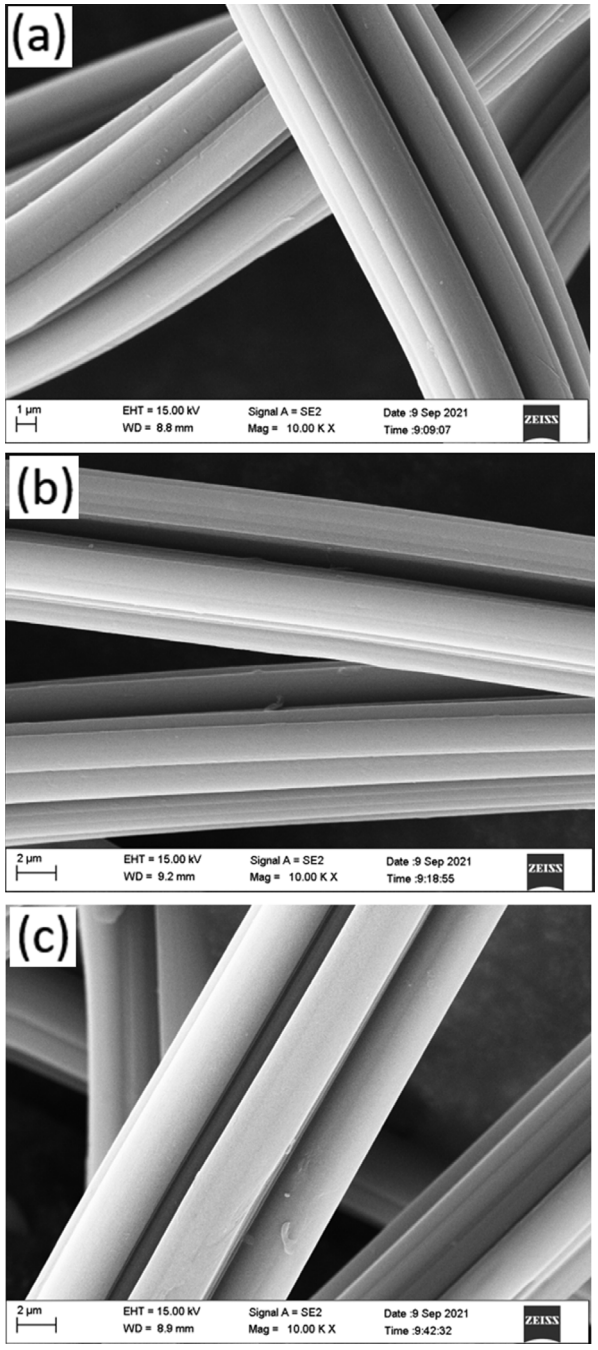

Fig. 3. SEM images of ACF (a), O-ACF (b), and O-ACF-PEI (5 : 2) (c).

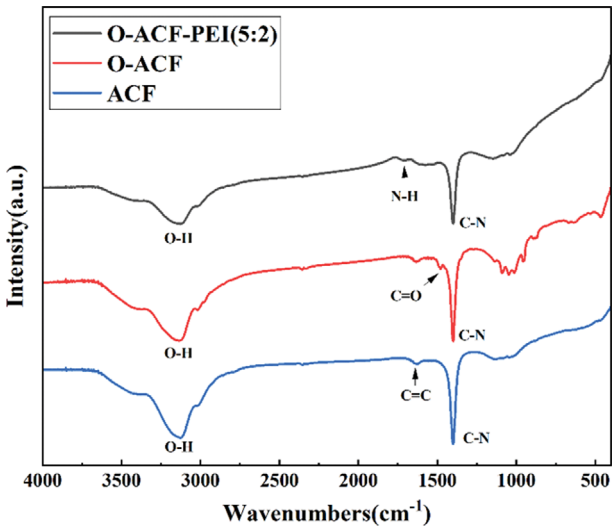

Fig. 4. FTIR spectra of ACF, O-ACF, and O-ACF-PEI (5 : 2).

ume is occupied by micropores and that the contribution of mesopores is smaller [25].

Through scanning electron microscopy analysis, the micromorphology of the ACF and modified samples can be observed. The integrity of the sample structure will directly affect its gas adsorption capacity. Fig. 3 shows that the original ACF material is a smooth fiber, and the modified sample maintains the original smooth appearance, which reveals that the modification did not destroy its integrity.

The FT-IR spectra of ACF, O-ACF and O-ACF-PEI (5 : 2) are shown in Fig. 4. It can be seen that the vibration band of ACF near 3,250 cm^{-1} is related to the stretching vibration of O-H, indicating the presence of hydroxyl groups. The vibration bands around 1,600 cm^{-1} and 1,350 cm^{-1} are attributed to C=C and C-N stretching vibrations, respectively [26]. A new vibration band appeared in O-ACF near 1,513 cm^{-1}, which is attributed to the appearance of C=O, indicating the successful oxidation of the ACF surface. O-ACF-PEI has a new vibration band near 1,695 cm^{-1}, which is attributed to the stretching vibration of N-H, indicating the presence of amine groups. The vibration zone is caused by the plane bending vibration of primary and secondary amines. The existence of the infrared characteristic peaks of these amines confirmed that PEI was loaded successfully in the ACF material.

To further verify the existence of amine groups, elemental analysis was performed on all samples. Table 2 summarizes the percentages of C, O, N, and H elements of the adsorbents before and after modification. Compared with ACF, the O element of O-ACF increased from 5.14% to 15.47%, indicating the successful oxidation of ACF. Compared with O-ACF, the N element of O-ACF-PEI (5 : 2) increased from 3.35% to 8.73% due to the addition of amine groups (NH_2), which further demonstrated the success of PEI on ACF load. We calculated the maximum value of the theoretical load PEI of ACF and O-ACF using formula 3-1. At the same time, the actual loading of PEI of O-ACF was determined by acid-base titration. Although the theoretical loading of O-ACF was 20%, only 12% of PEI was actually loaded, which was due to the pore volume of O-ACF. The size limits the amount of PEI's payload.

$$n = \frac{v}{v + \rho} \tag{1}$$

where n (%) is the maximum proportion of theoretically loaded PEI, v (cm^3/g) is the pore volume per gram of adsorbent, ρ (g/cm^3)

Table 2. ICP data and PEI loading for the adsorbents

Samples	C (%)	N (%)	O (%)	H (%)	PEI actual load (%)	PEI maximum load (%)
ACF	92.7	1.68	5.14	0.48	-	31
O-ACF	80.4	3.35	15.47	0.78	-	20
O-ACF-PEI (5 : 2)	77.3	8.73	13.16	0.81	12	20

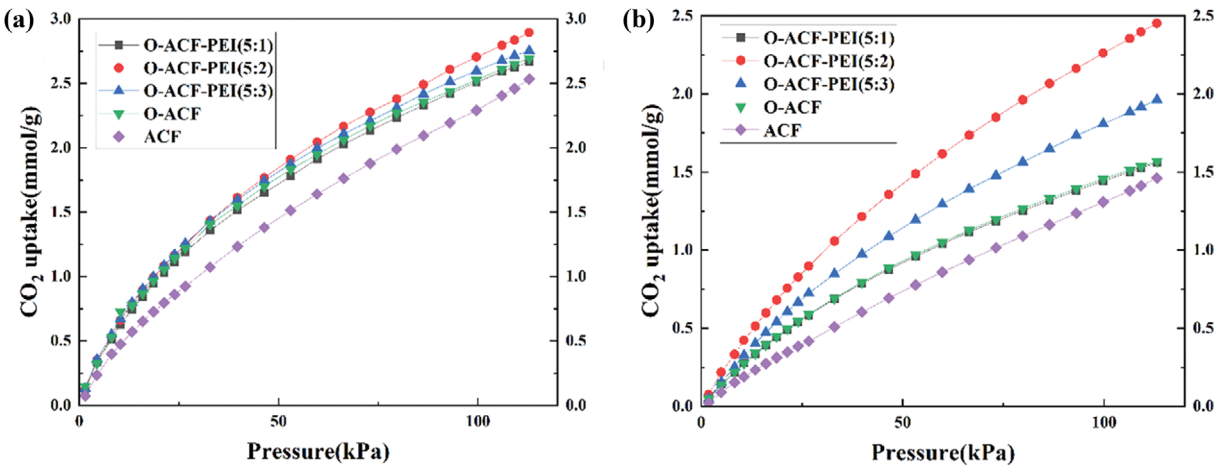

Fig. 5. CO_2 adsorption isotherms of synthesized adsorbents at 303 K (a) and 333 K (b).

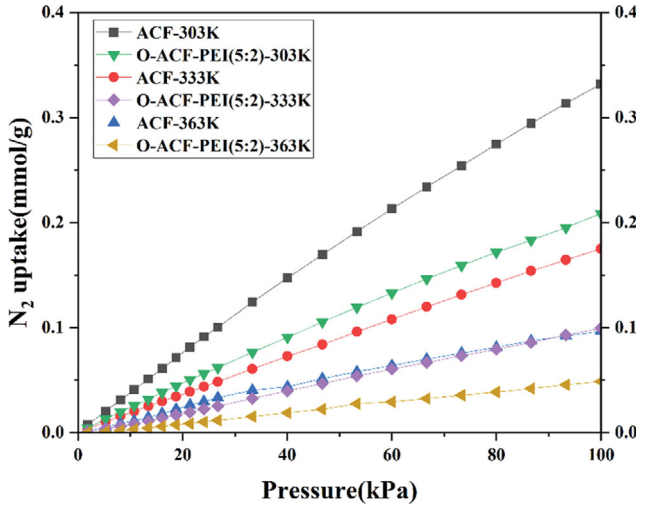

Fig. 6. N_2 adsorption isotherms of ACF and O-ACF-PEI (5 : 2) at different temperatures.

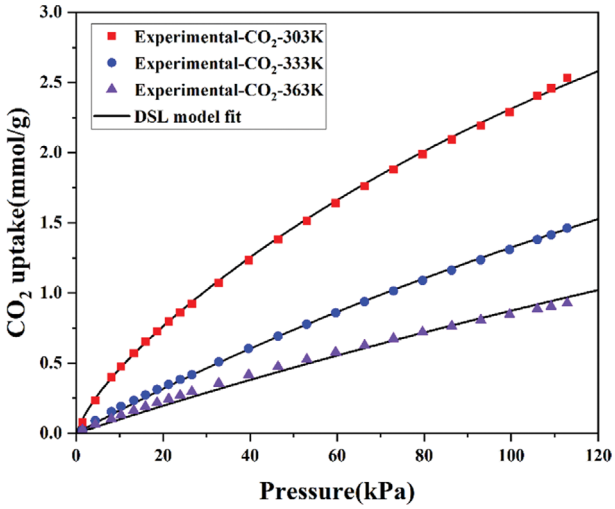

Fig. 7. Dual-site Langmuir fitting curves of ACF CO_2 adsorption isotherms at different temperatures.

is the density of PEI; it is known that ρ_{PEI}=1.03 g/cm^3, v_{ACF}=0.461 cm^3/g, $v_{O\text{-}ACF}$=0.257 cm^3/g, calculated n_{ACF}=31%, $n_{O\text{-}ACF}$=20%.

2. Adsorption Studies

2-1. Effect of Temperature on CO_2 Adsorption

The CO_2 adsorption capacities of the original adsorbent ACF, oxidized O-ACF and modified adsorbents O-ACF-PEI (5 : 1), O-ACF-PEI (5 : 2), and O-ACF-PEI (5 : 3) at different temperatures are shown in Fig. 5. In the figures, we can see that the CO_2 adsorption capacity of all adsorbents increases with increasing pressure, which conforms to the type I adsorption isotherm. However, as the temperature increases (from 303 to 333 K), the CO_2 adsorption capacity of all samples decreases (2.91 to 2.45 mmol/g and 2.53 to 1.46 mmol/g), which refers to physical adsorption including exothermic processes. A higher temperature will provide more kinetic energy for the CO_2 molecules, thereby increasing their ability to eliminate adsorption, resulting in a decrease in the binding between the CO_2 molecules and the adsorbent surface [27].

2-2. Effect of Temperature on N_2 Adsorption

To study the N_2 adsorption performance of activated carbon fibers before and after modification, N_2 adsorption tests were performed on ACF and O-ACF-PEI (5 : 2). The N_2 adsorption performance was tested at 303 K, 333 K and 363 K to explore the N_2 adsorption capacity at different temperatures. Fig. 6 shows the N_2 adsorption isotherms of ACF and O-ACF-PEI (5 : 2) at different temperatures. It can be seen that the adsorption amount of N_2 by ACF and O-ACF-PEI (5 : 2) increases with the increase of temperature, and the effect of temperature is consistent with the effect on CO_2 adsorption on the whole. From 303 K to 363 K, the adsorption capacity of ACF decreased from 0.3 mmol/g to 0.1 mmol/g, and the adsorption capacity of O-ACF-PEI (5 : 2) decreased from 0.2 mmol/g to 0.05 mmol/g, indicating that the N_2 adsorption capacity of the modified adsorbent was lower.

2-3. CO_2 and N_2 Adsorption Curve Fitting

To explore the adsorption equilibrium relationship between the adsorbent and the adsorbate, it is necessary to model the experimental data to provide a certain theory for application in other environments. In this study, the CO_2 and N_2 adsorption curves of the original ACF material and the modified O-ACF-PEI (5 : 2) material at three temperatures of 303 K, 333 K and 363 K were fitted by dual-site Langmuir (DSL) and Langmuir models, and the degree of fit between the experimental data and the model was analyzed.

2-3-1. Dual-site Langmuir (DSL) Model Fitting

The dual-site Langmuir (DSL) adsorption model considers the heterogeneous adsorbent surface formed by two sites with different characteristic adsorption energies [28]. That is, it is assumed that the adsorbent has two different adsorption sites for the adsorbed gas so that the adsorption process can be described more accurately. The equation of the DSL model is [29]:

$$q = \frac{q_1 b_1 p}{1 + b_1 p} + \frac{q_2 b_2 p}{1 + b_2 p} \tag{2}$$

$$b_i = b_{0i} \exp\left(\frac{\Delta H_i}{RT}\right) \tag{3}$$

where q is the adsorption capacity under equilibrium pressure (mmol/g), q_1 and q_2 are the ideal maximum adsorption capacities (mmol/g), b_i and b_{0i} are the adsorption constants of the two adsorption sites, p is the variable pressure (kPa), ΔH is the heat of

Table 3. Fitting parameters and coefficients of the DSL model

Model	Adsorbent	Fitting parameters						Fitting coefficient
DSL	ACF	q_1	b_{01}	ΔH_1	q_2	b_{02}	ΔH_2	R^2
		6.4763	6.32E-6	16628	0.2731	5.9E-62	350697	0.9983

adsorption (J/mol), R is the ideal gas constant (8.314 J/mol·K), and T is the adsorption temperature (K).

The fitting of the CO_2 adsorption isotherm of ACF at three temperatures of 303 K, 333 K, and 363 K is shown in Fig. 7, and the fitting parameters and fitting correlation coefficients are shown in Table 2. It can be seen that the dual-site Langmuir model has a good degree of fit, and the fitting correlation coefficients at the three temperatures are all high, which can describe the adsorption curve well.

2-3-2. Langmuir Model Fitting

The Langmuir model generally defaults to the uniform surface of the adsorbent, and the adsorption of the solid adsorbent surface is single-layer [28]. In addition, the Langmuir model believes that the adsorbent adsorbs and desorbs at the same time in the process of adsorbing gas and reaches adsorption equilibrium within a certain period of time. The Langmuir model equation is [30]:

$$q = \frac{q_s bp}{1+bp} \tag{4}$$

$$b = b_0 \exp\left(\frac{\Delta H}{RT}\right) \tag{5}$$

q is the adsorption capacity under equilibrium pressure (mmol/g), q_s is the ideal maximum adsorption capacity (mmol/g), b and b_0 are the adsorption equilibrium constants, p is the variable pressure (kPa), ΔH is the heat of adsorption (J/mol), R is the ideal gas constant (8.314 J/mol·K), and T is the adsorption temperature (K).

The fitting of N_2 adsorption isotherms of ACF and O-ACF-PEI (5 : 2) at three temperatures of 303 K, 333 K, and 363 K is shown in Fig. 8. The fitting parameters and fitting correlation coefficients are shown in Table 4. In the figure and table, it can be seen that the Langmuir model has a higher degree of fit to ACF than to O-ACF-PEI (5 : 2). The Langmuir model has a good degree of fit for the adsorption point of ACF at three temperatures, but the Langmuir model slightly deviates from the adsorption point of O-ACF-PEI (5 : 2) at 303 K. The fitting curve coincides well with the adsorption point under normal pressure, but as the pressure increases, the fitting curve gradually deviates from the actual adsorption point, and the description of the adsorption trend is inaccurate.

2-3-3. Selectivity of CO_2/N_2 Adsorption and the Isosteric Heat of Adsorption

The adsorption selectivity affects the adsorption of a specific gas by the adsorbent, so an in-depth study on the CO_2/N_2 adsorption selectivity was conducted. The main method currently used to explore the adsorption selectivity of solid adsorbents is to use the ideal solution adsorption theory (IAST) model to make predictions. IAST uses experimental or simulated data to predict the adsorption isotherms of multiple components in microporous materials. The IAST model equation is:

$$s = \frac{q_i/q_j}{p_i/p_j} \tag{6}$$

where S is the selectivity coefficient, q_i and q_j are the adsorption capacities of component *i* (CO_2) and component *j* (N_2), respectively, and p_i and p_j are the partial pressures of component *i* (CO_2) and component *j* (N_2), respectively.

The main research in this study is the adsorption and separation of CO_2 from the flue gas of a power plant. Generally, 73-77% N_2 is present in the flue gas of a power plant after combustion [31]. Assuming that the power plant flue gas contains 25% CO_2 and 75%

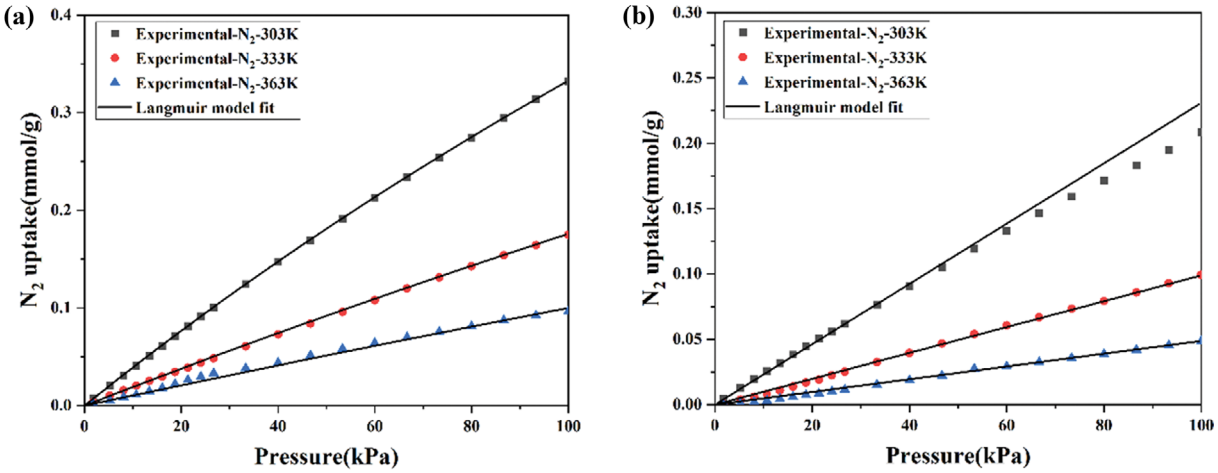

Fig. 8. Langmuir fitting curves of ACF (a) and O-ACF-PEI (5 : 2) (b) N_2 adsorption isotherms at different temperatures.

Table 4. Fitting parameters and coefficients of the Langmuir model

Model	Adsorbent	Fitting parameters			Fitting coefficient
		q_s	b_0	ΔH	R^2
Langmuir	ACF	2.045	6.23E-7	20,267.5	0.9988
	O-ACF-PEI (5 : 2)	206,515	9.13E-13	23,713.6	0.9926

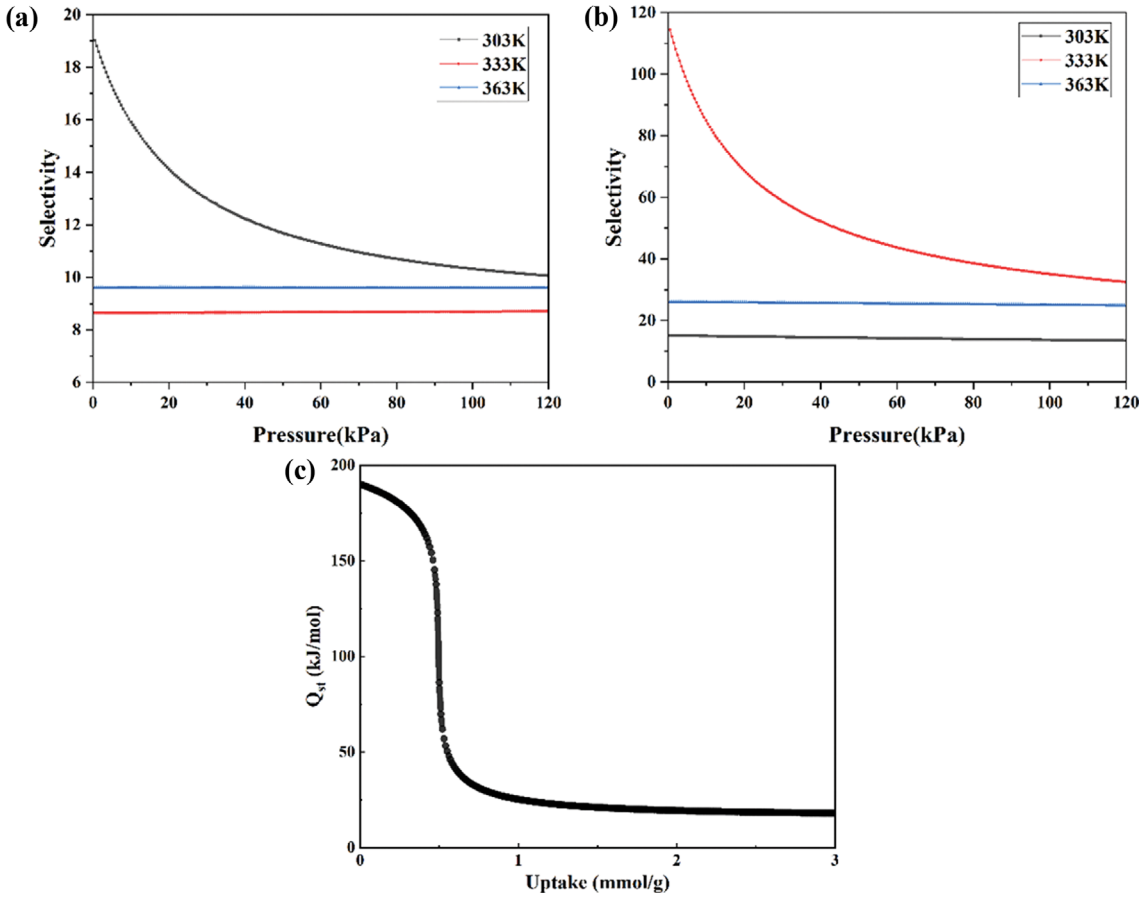

Fig. 9. CO_2/N_2 selectivity of ACF (a) and O-ACF-PEI (5 : 2) (b) at different temperatures; CO_2 isosteric heat curve of O-ACF-PEI (5 : 2) (c).

N_2, the partial pressures of component *i* (CO_2) and component *j* (N_2) are taken as 0.25 and 0.75 when the IAST model is used for prediction. Fig. 9 shows the CO_2/N_2 adsorption selective ratio curves of ACF and O-ACF-PEI (5 : 2). We can see that the adsorption selectivity ratios of ACF at 303 K and O-ACF-PEI (5 :2) at 333 K both decrease with increasing adsorption pressure and gradually become flat. This is because the CO_2 adsorption isotherms of ACF at 303 K and O-ACF-PEI (5 : 2) at 333 K are type I Langmuir isotherms. The adsorption capacity increases rapidly in the low-pressure section and slowly increases in the high-pressure section, while the N_2 adsorption isotherms are all similar to a straight line, and the adsorption capacity increases linearly with increasing adsorption pressure.

In addition, the isosteric heat of adsorption is one of the important parameters to measure the performance of the adsorbent. In the adsorption process, when the gas molecules move to the surface of the adsorbent and combine, the molecular motion will be greatly reduced, thereby releasing a certain amount of heat. Fig. 9(c) shows the CO_2 isosteric heat curve of O-ACF-PEI (5 : 2). When the CO_2 adsorption is approximately equal to 0, the initial isothermal heat is 189 kJ/mol. As the adsorption capacity increases, the isosteric heat first decreases slowly, then decreases quickly, and finally slowly drops to 22 kJ/mol again. The very high isosteric heat of adsorption at the beginning of adsorption can be attributed to chemisorption occurring at the beginning of adsorption, and the heat released by chemisorption is much higher than that of physical adsorption. With the saturation of chemisorption, the isosteric heat of adsorption begins to decrease rapidly until it drops to 22 kJ/mol, which indicates that physical adsorption is taking place in the final stage.

2-4. Adsorption Thermodynamics

The adsorption thermodynamic parameters, free Gibbs energy changes (ΔG), enthalpy changes (ΔH) and entropy change (ΔS), can be determined by the following equations [32,33]:

$$\Delta G = -RT\ln K_L \quad (7)$$

$$\Delta G = \Delta H - T\Delta S \quad (8)$$

where R is the ideal gas constant, (8.314 J/mol·K); T is the thermodynamic temperature, (K); K_L is the Langmuir constant.

The adsorption thermodynamic parameters are shown in Table

Table 5. Thermodynamic parameters for the adsorption of CO_2 on O-ACF-PEI (5 : 2)

Adsorbent	T	ΔG	ΔH	ΔS
	K	kJ/mol	kJ/mol	kJ/mol·K
O-ACF-PEI (5 : 2)	303	−7.5142	−23.3247	−0.0522
	333	−5.9487		
	363	−4.3834		

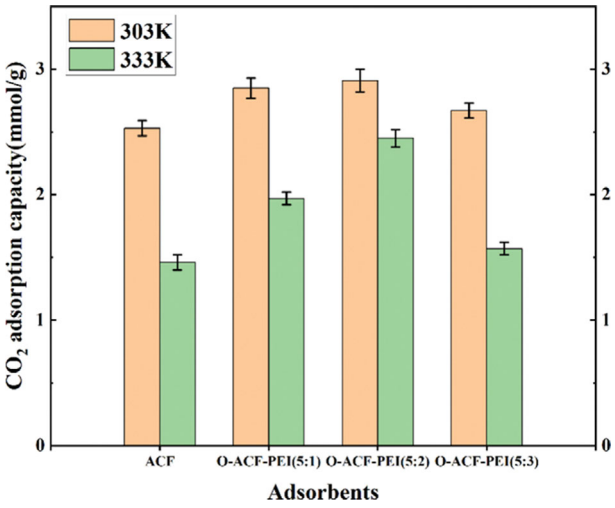

Fig. 10. Effect of PEI loading on CO_2 adsorption by the samples.

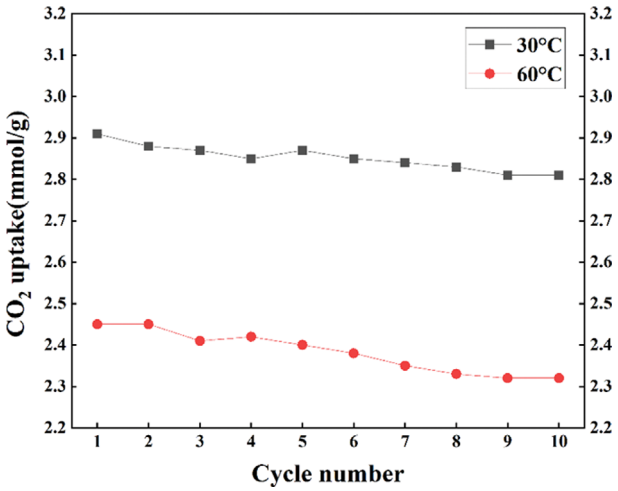

Fig. 11. Cyclic adsorption of O-ACF-PEI (5 : 2) at different temperature.

5. When the modified adsorbent is adsorbed at different temperatures, the free Gibbs energy change ΔG is negative, indicating that the adsorption is feasible and spontaneous. The absolute value of ΔG decreases with the increase of temperature, indicating that higher temperature is not conducive to CO_2 adsorption, which has also been verified in the previous experiments. The enthalpy change ΔH is negative, indicating that the adsorption process is exothermic. The entropy change ΔS is negative, indicating that the degree of confounding of the system decreases during the adsorption process, and CO_2 molecules migrate from the gas phase host to the active sites on the adsorbent surface, which leads to a decrease in the entropy value of the system.

2-5. Influence of Amine Loading

The effects of PEI loading on CO_2 adsorption by using as-synthesized samples are shown in Fig. 10. The results indicate that as the amount of PEI increases, the CO_2 adsorption capacity of the adsorbent first increases and then decreases. The adsorption capacity of ACF was measured as only 2.53 mmol/g and 1.46 mmol/g, respectively, at 303 to 333 K, probably due to weak physisorption of CO_2. However, it could be observed that the adsorption capacities of O-ACF-PEI (5 : 1) and O-ACF-PEI (5 : 2) for CO_2 were quite impressive with values of 2.91 to 2.53 and 2.45 to 1.46 mmol/g, respectively, at 303 to 333 K. The highest CO_2 adsorption capacity after loading PEI was 1.7 times that of the original material. This is because after ACF is loaded with PEI, it not only physically adsorbs carbon dioxide but also chemically adsorbs it, so the amount of CO_2 adsorbed by ACF is increased. This confirms that amine groups play a major role in the enhancement of CO_2 adsorption by a huge margin. However, the adsorption amount of higher amine-loaded sample (O-ACF-PEI (5 : 3)) shows some decrease in the adsorption amount, respectively, at 303 to 333 K. This is because the excessive organic amine in the adsorbent blocks the pores of ACF, causing CO_2 molecules to not enter the pores. Similar results were also observed in many previous studies [34,35].

2-6. Regeneration of Adsorbent

In practical applications, the adsorbent should not only have high CO_2 adsorption capacity and high selectivity, but also exhibit a stable cycle regeneration capability. Fig. 11 shows the adsorption capacity of the adsorbent O-ACF-PEI (5 : 2) at 30 and 60 °C for 10 cycles. The desorption condition of the adsorbent is 120 °C for 6 hours. Cyclic data shows that the CO_2 adsorption capacity of the modified adsorbent decreases by 3.4% and 5.3% at 30 and 60 °C, respectively, which indicates that the regeneration performance of the adsorbent is relatively stable.

Table 6. Comparison of O-ACF-PEI (5 : 2) with other amine-modified adsorbents

Support	Functionalization	Adsorption capacity (mmol/g) for CO_2	T (K)	Reference
Resin HP20	PEI-50	4.11	298	[36]
MC	PEI	2.25	298	[37]
Zeolite 13X	PEI	0.25	298	[38]
Zeolite 5A	PEI	5.05	298	[39]
MCM-41	Ethanolamine	2.26	298	[40]
MgO-SiO_2 nanofibers	PEI	2.48	348	[41]
Halloysite	PEI	2.75	353	[42]
Mesoporous carbon	PEI	4.70	333	[43]
ACF	PEI	2.45	333	This study

2-7. Comparison of Performance with other Amine-modified Adsorbents

The CO_2 adsorption capacity of the modified O-ACF-PEI adsorbent is compared with the performance of other amine-modified adsorbents reported in the literature as shown in Table 6. Many kinds of amine and carrier adsorbents have been used to capture CO_2, but the synthesis methods of most adsorbents are complicated and expensive. The synthesized O-ACF-PEI adsorbent in this experiment has the characteristics of simple synthesis, large high-temperature adsorption capacity and high selectivity, which can be used to capture CO_2 in high temperature flue gases of power plants.

CONCLUSIONS

We improved the CO_2 adsorption capacity by loading the organic amine PEI into oxidized activated carbon fiber. First, ACF was oxidized with nitric acid and sulfuric acid (1 : 3, V/V), and then PEI was loaded into the oxidized ACF. The FT-IR analysis revealed new peaks of C=N, which confirmed the successful binding of polyethylimine molecules on the parent material. The XRD analysis revealed that the structure of ACF remained intact even after the modification process of ACF. SEM analysis indicated that amine loading did not affect the integrity of ACF. The adsorption results showed that under the conditions of 333 K and 1 bar, when ACF : PEI (m/m) was 5 : 2, the CO_2 adsorption capacity was the largest, increasing from 1.5 mmol/g to 2.5 mmol/g, which represented an increase of 68%. At the same time, the dual site Langmuir and the Langmuir isotherm models fitted the experimental data of synthetic adsorbents well. We also calculated through the IAST method that the selectivity of CO_2 adsorption to N_2 adsorption increased from 18 to 119. The conclusion of this study is that polyethyleneimine-modified activated carbon fiber would be a promising adsorption material with excellent potential for CO_2 separation from high temperature post-combustion flue gases.

ACKNOWLEDGEMENTS

This work was financially supported by the Fundamental Research Funds for Central Universities (grant number N182508027), the National Natural Science Foundation of China (grant number 22078054), and the science and technology project of Liaoning province (2021JH1/10400011).

REFERENCES

1. M. M. Halmann and M. Steinberg, *Greenhouse gas carbon dioxide mitigation: Science and technology [M]*, Boca Raton, Florida: Lewis Publishers (1999).
2. E. Monnin, A. Indermuhle, A. Dallenbach, J. Fluckiger, B. Stauffer, T. F. Stocker, D. Raynaud and J.M. Barnola, *Science*, **291**, 112 (2001).
3. Z. Li, S. Chen, D. Hopkinson and D. Luebke, *Int. J. Greenh. Gas Con.*, **44**, 59 (2016).
4. M. K. Mondal, H. K. Balsora and P. Varshney, *Energy*, **46**, 431 (2012).
5. E. Favre, *Chem. Eng. J.*, **171**, 782 (2011).
6. IPCC, *Carbon dioxide capture and storage [M]*, Cambridge: United Kingdom (2005).
7. Y. E. Kim, J. H. Park, S. H. Yun, S. C. Nam, S. K. Jeong and Y. I. Yoon, *J. Ind. Eng. Chem.*, **20**(4), 1486 (2014).
8. J. Zhou and W. S. Ho, *Membr. Sci.*, **286**, 310 (2006).
9. S. Choi, J. H. Drese and C. W. Jones, *ChemSusChem.*, **2**, 796 (2009).
10. N. Goyal, V. K. Bulasara and S. Barman, *J. Hazard. Mater.*, **344**, 417 (2018).
11. N. Goyal, S. Barman and V. K. Bulasara, *Micropor. Mesopor. Mater.*, **259**, 184 (2018).
12. A. G. Pandolfo, M. Amini-amoli and J. S. Killingley, *Carbon*, **32**(5), 1015 (1994).
13. A. Serbezov, *Chem. Eng. Data*, **48**, 412 (2003).
14. B. Chen, M. Eddaoudi and S. T. Hyde, *Science*, **291**, 1021 (2001).
15. L. R. Nathaniel, E. Juergen and E. Mohamed, *Science*, **300**, 1127 (2003).
16. H. K. Chael, D. Y. Siberio-Perez and J. Kim, *Nature*, **427**, 523 (2004).
17. Y. L. Xu, R. Wang, J. Y. Wang, J. H. Li, T. F. Jiao and Zh. F. Liu, *Chem. Eng. J.*, **417**, 129233 (2021).
18. Z. H. Rada, H. R. Abid, H. Sun, J. Shang, J. Li, Y. He, S. Liu and S. Wang, *Pro. Nat. Sci. Mater. Int.*, **28**, 160 (2018).
19. S. K. Ryu, *High Temp. High Pressure*, **22**, 345 (1990).
20. D. F. Quinn and J. A. Macdonald, *Carbon*, **30**, 1097 (1992).
21. R. Guo, T. F. Jiao, R. F. Li, Y. Chen, W. Ch. Guo, L. X. Zhang, J. X. Zhou, Q. R. Zhang and Q. M. Peng, *ACS Sustainable Chem. Eng.*, **6**, 1279 (2018).
22. R. R. Xing, W. Wang, T. F. Jiao, K. Ma, Q. R. Zhang, W. Hong, H. Qiu, J. X. Zhou, L. X. Zhang and Q. M. Peng, *ACS Sustainable Chem. Eng.*, **5**, 4948 (2017).
23. X. Guo, H. Huang, D. Liu and C. Zhong, *Chem. Eng. Sci.*, **189**, 277 (2018).
24. A. Huang and B. Feng, *Int. J. Hydrogen Energy*, **43**, 2224 (2018).
25. D. Peredo-Mancilla, C. M. Ghimbeuc, B. N. Ho, M. Jeguirim, C. Hort and D. Bessieres, *J. Environ. Chem. Eng.*, **7**, 103 (2019).
26. X. G. Li, F. Wei, M. R. Huang and Y. B. Xie, *J. Phys. Chem.*, **B111**, 5829 (2007).
27. F. Raganati, M. Alfe, V. Gargiulo, R. Chirone and P. Ammendol, *Chem. Eng. Res. Des.*, **134**, 540 (2018).
28. A. Awadallah-F, F. Hillman, S. A. Al-Muhtaseb and H.K. Jeong, *Ind. Eng. Chem. Res.*, **58**(16), 6653 (2019).
29. X. Tang, N. Ripepi, Y.-H. Kim, N. P. Stadie, L. J. Yu and M. R. Hall, *Fuel*, **185**, 10 (2016).
30. Y. Park, D. K. Moon, Y. H. Kim, H. Ahn and C. H. Lee, *Adsorption*, **20**(4), 631 (2014).
31. L. Yang, L. Jing, Y. S. Lin and C. Ming, *J. of Phys. Chem. C*, **118**(13), 6744 (2015).
32. O. Gercel, A. Ozcan, A. S. Ozcan and H. F. Gercel, *Appl. Surf. Sci.*, **253**, 4843 (2007).
33. J. J. Kong, Q. Y. Yue, L. H. Huang, Y. Gao, Y. Y. Sun, B. Y. Gao, Q. Li and Y. Wang, *Chem. Eng. J.*, **221**, 62 (2013).
34. A. Abbasi, M. M. Nasef, S. Kheawhom, R. Faridi-Majidic, M. Takeshid, E. Abouzari-Lotfe and T. Choong, *Radiat. Phys. Chem.*, **156**, 58 (2019).
35. A. R. Sujan, S. H. Pang, G. Zhu, C. W. Jones and R. P. Lively, *ACS Sustain. Chem. Eng.*, **7**, 5264 (2019).
36. Z. H. Chen, S. B. Deng, H. R. Wei, B. Wang, J. Huang and G. Yu, *ACS Appl. Mater. Interfaces*, **5**, 6937 (2013).

37. J. Wang, H. Huang, M. Wang, L. Yao, W. Qiao, D. Long and L. Ling, *Ind. Eng. Chem. Res.*, **54**, 5319 (2015).
38. C. Chen, S. S. Kim, W. S. Cho and W. S. Ahn, *Appl. Surf. Sci.*, **332**, 167 (2015).
39. L. H. Zhou, J. Xu, F. Gao, X. W. Liu and J. Hu, *Micropor. Mesopor. Mater.*, **222**, 113 (2016).
40. S. Mukherjee, A. Amar and N. Samanta, *Adv. Powder Technol.*, **30**, 3231 (2019).
41. J. Ouyang, W. Gu, C. Zheng, H. Yang, X. Zhang, Y. Jin, J. Chen and J. Jiang, *Appl. Clay Sci.*, **152**, 267 (2018).
42. M. Niu, H. Yang, X. Zhang, Y. Wang and A. Tang, *ACS Appl. Mater. Interfaces*, **8**, 17312 (2016).
43. H. Wang, H. Chen, X. Zhou, X. Liu, W. Qiao, D. Long and L. Ling, *J. Environ. Sci.*, **25**, 124 (2013).